Supporting Information

Development of Dual-nanoarchitecture Photoanodes Based on Microwave-assisted $ZnS(en)_{0.5}$ Nanoplates for Photoelectrochemical Hydrogen Generation

Ruturaj P. Patil[⊥,†], *Mahadeo A. Mahadik*[⊥,†], *Weon-Sik Chae*[*,‡], *Jungho Ryu*[*,§], and *Jum Suk Jang*[*,†]

[†]*Division of Biotechnology, Safety, Environment and Life Science Institute, College of Environmental and Bioresource Sciences, Jeonbuk National University, Iksan, 54596, Republic of Korea*

[‡]*Daegu Center, Korea Basic Science Institute, Daegu 41566, Republic of Korea*

[§]*Geologic Environment Research Division, Korea Institute of Geoscience and Mineral Resources (KIGAM), Daejeon 34132, Republic of* Korea

[*]Corresponding Author's Email: wschae@kbsi.re.kr (WSC); jryu@kigam.re.kr (JR); jangjs75@jbnu.ac.kr (JSJ)

Table S1. XPS Atomic Composition of $ZnS(en)_{0.5}$ NP -2 electrode.

Element	$ZnS(en)_{0.5}$ -2
C1s	32.49
O1s	12.18
Zn 2p	17.43
S 2p	12.72
N 1S	25.18

Table S2. Calculated resistance and capacitance values for Nyquist plots of (a) $Zn_{1-x}Cd_xS$ PNP/ZnO NR160 and (b) $Zn_{1-x}Cd_xS$ PNP/ZnO NR180 photoanodes.

Samples	R_s	R_{ct1}	R_{ct2}	CPE1	CPE2
	Ω	Ω	Ω	μF	μF
(a)	3.77	79.79	432	378	1153
(b)	3.81	84.32	464	724	560

Table S3. PL lifetime parameters of (a) $Zn_{1-x}Cd_xS$ PNP/ZnO NR160 and (b) $Zn_{1-x}Cd_xS$ PNP/ZnO NR180 photoanodes.

Sample	λ_{ex} (nm)	λ_{det} (nm)	A_1 (%)	τ_1 (ns)	A_2 (%)	τ_2 (ns)	A_3 (%)	τ_3 (ns)	A_4 (%)	τ_4 (ns)	$<\tau>^{a)}$ (ns)
(a)	375	415	99.9	0.20	0.1	5.0	–	–	–	–	0.38
		550	57.8	0.95	33.2	3.7	8.9	12	0.1	147	13
	470	750	93.5	2.6	5.0	79	1.1	1094	0.4	12727	9245
(b)	375	415	99.9	0.26	0.1	5.9	–	–	–	–	0.39
		550	74.7	0.6	21.9	3.0	3.1	16	0.3	288	94
	470	750	93.3	1.5	5.4	67	1.1	914	0.2	9030	5544

Time-resolved PL intensity defined by $I(t) = \sum_j A_j e^{-t/\tau_j}$, where *I(t)* describes emission intensity as a function of time, *A* denotes the amplitude, and τ indicates PL lifespan. [a)]Average lifespan was calculated using the following equation: $<\tau> = \sum_j A_j \tau_j^2 / \sum_j A_j \tau_j$.

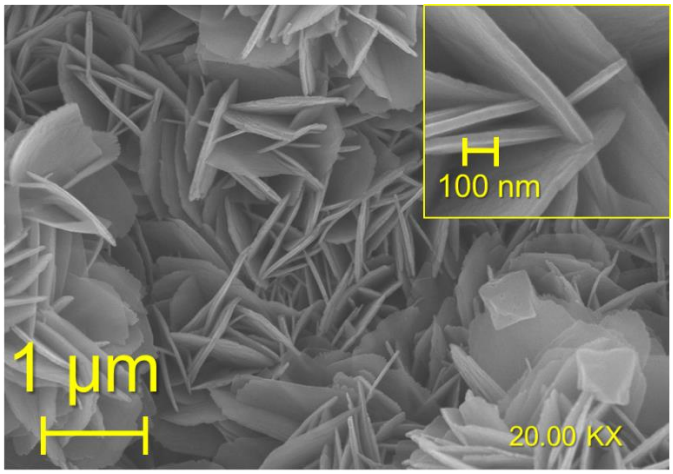

Figure S1. Top view of FESEM images and magnified view (inset) of $ZnS(en)_{0.5}$ NP –1.5 electrode.

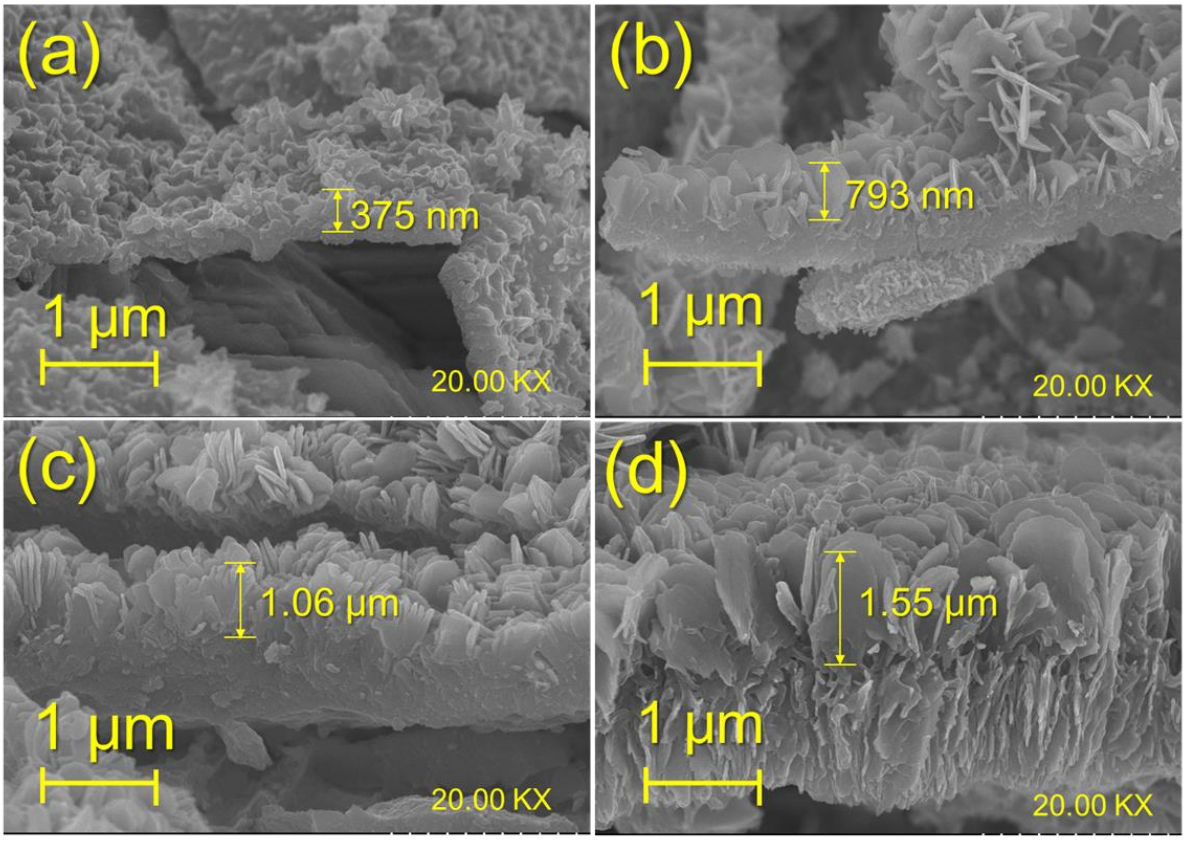

Figure S2. FESEM images (cross section) of (a) $ZnS(en)_{0.5}$ NP -0.5, (b) $ZnS(en)_{0.5}$ NP -1, (c) $ZnS(en)_{0.5}$ NP -1.5, and (d) $ZnS(en)_{0.5}$ NP -2 electrodes.

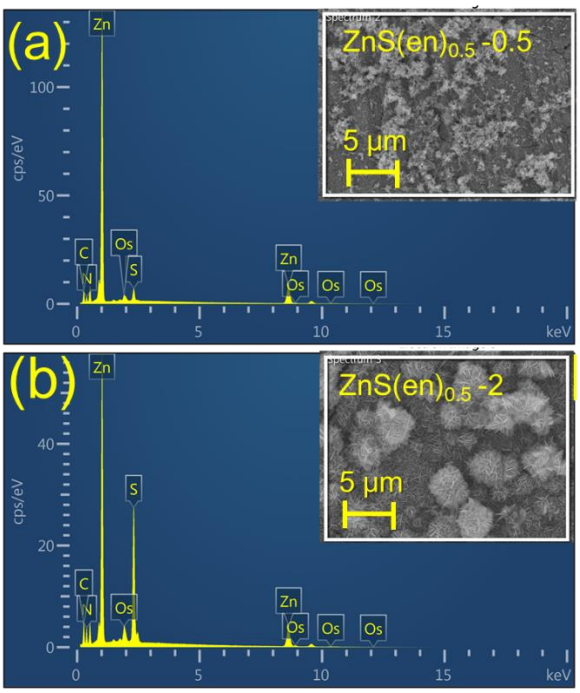

Element	Wt%	Wt% Sigma	Atomic %
C	17.62	0.27	44.82
N	8.94	0.24	19.51
S	2.76	0.04	2.63
Zn	70.68	0.32	33.04
Total:	100.00		100.00

Element	Wt%	Wt% Sigma	Atomic %
C	21.11	0.36	42.32
N	16.73	0.34	28.76
S	15.78	0.14	11.85
Zn	46.38	0.38	17.08
Total:	100.00		100.00

Figure S3. FESEM EDAX of inorganic –organic (a) $ZnS(en)_{0.5}$ NP -0.5 and (b) $ZnS(en)_{0.5}$ NP -2 electrode.

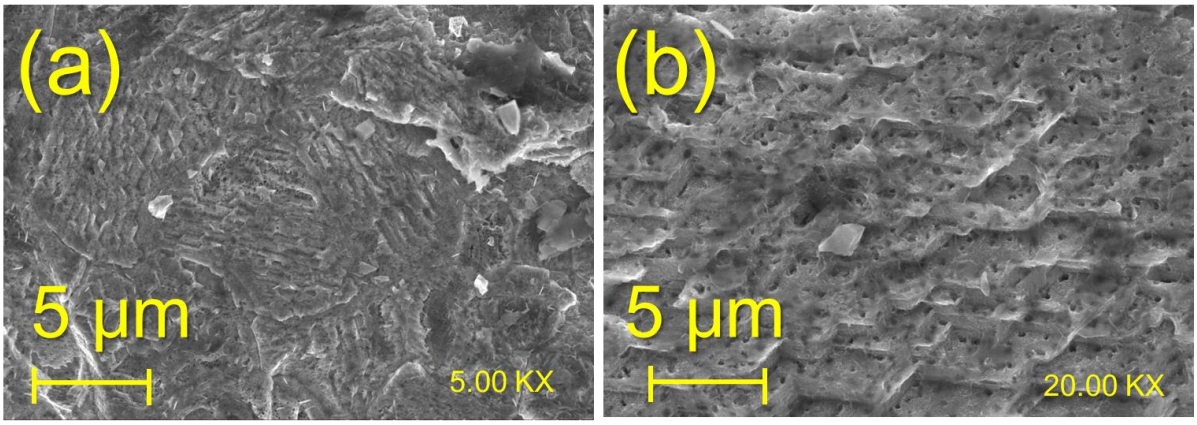

Figure S4. (a-b) FESEM images of $ZnS(en)_{0.5}$ NP -2 electrode (without Zn source).

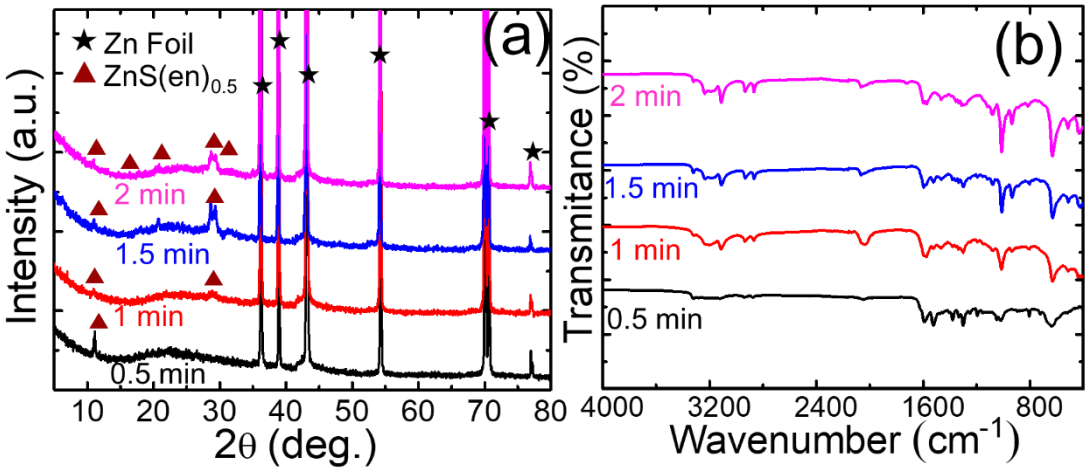

Figure S5. (a) XRD and (b) FTIR spectra of inorganic-organic $ZnS(en)_{0.5}$ NP -0.5, $ZnS(en)_{0.5}$ NP -1 min, $ZnS(en)_{0.5}$ NP -1.5, and $ZnS(en)_{0.5}$ NP -2 electrodes (Zn foil: JCPDS No. 87-0713).

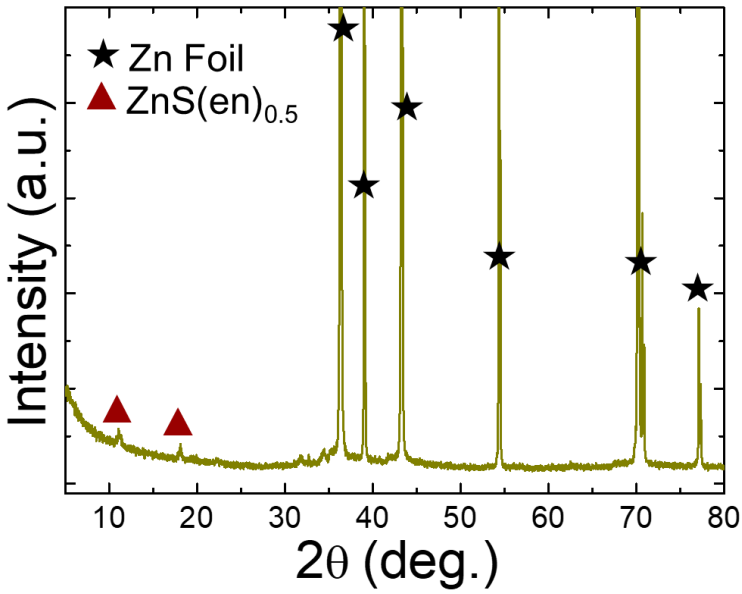

Figure S6. XRD pattern of inorganic-organic $ZnS(en)_{0.5}$ NP -2 electrode (without Zn source), (Zn foil: JCPDS No. 87-0713).

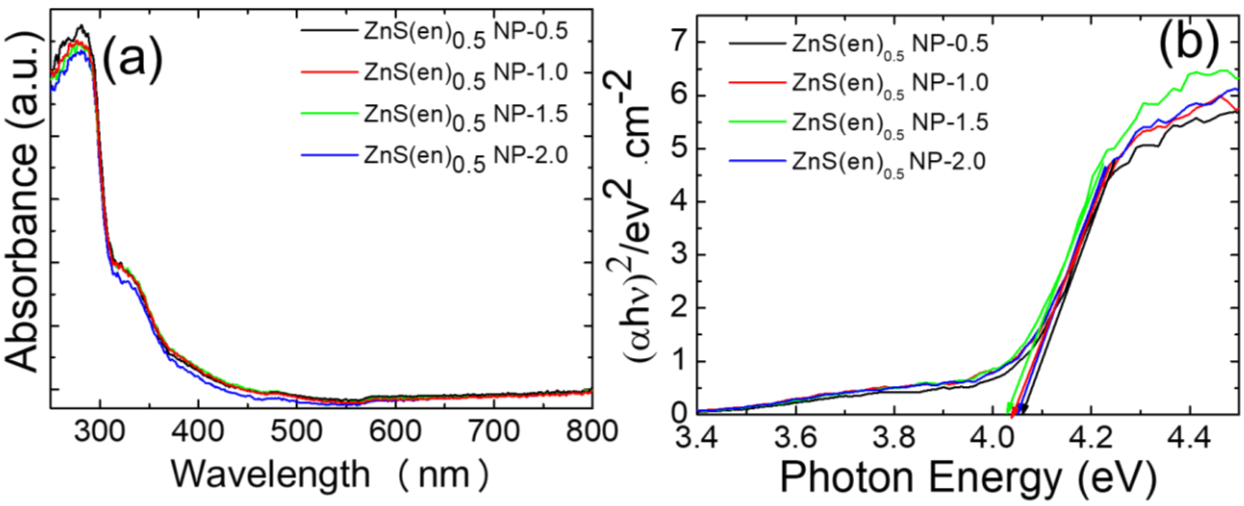

Figure S7. (a) UV-Vis and (b) band gap of $ZnS(en)_{0.5}$ NP -0.5, $ZnS(en)_{0.5}$ NP -1 , $ZnS(en)_{0.5}$ -1.5 and $ZnS(en)_{0.5}$ NP -2 electrodes.

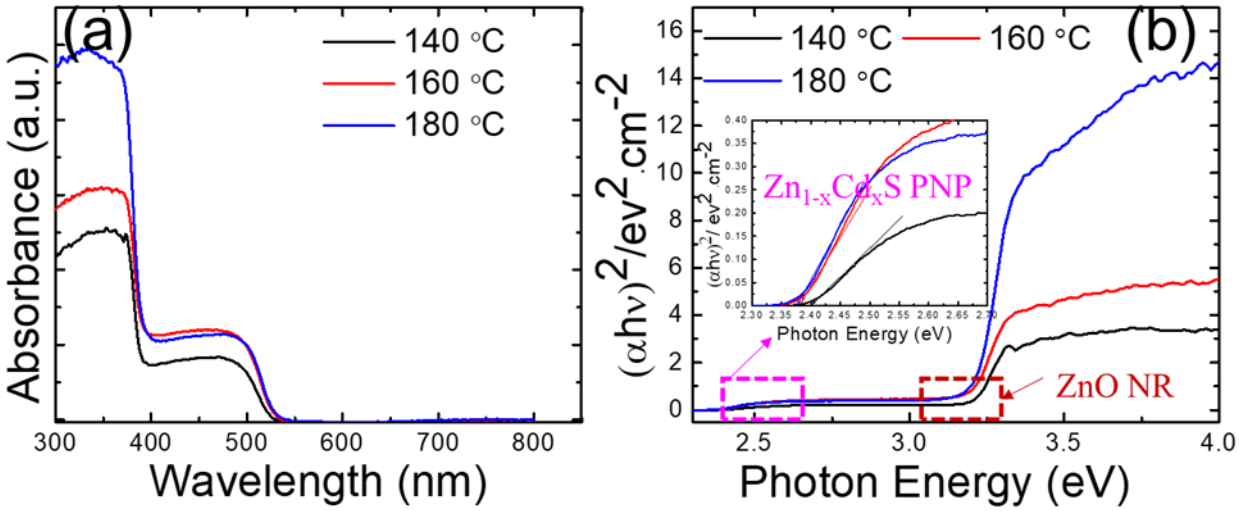

Figure S8. (a) UV-Vis and (b) bandgap of $Zn_{1-x}Cd_xS$ PNP/ ZnO NR140 , $Zn_{1-x}Cd_xS$ PNP/ ZnO NR160, and $Zn_{1-x}Cd_xS$ PNP/ ZnO NR180 photoanodes.

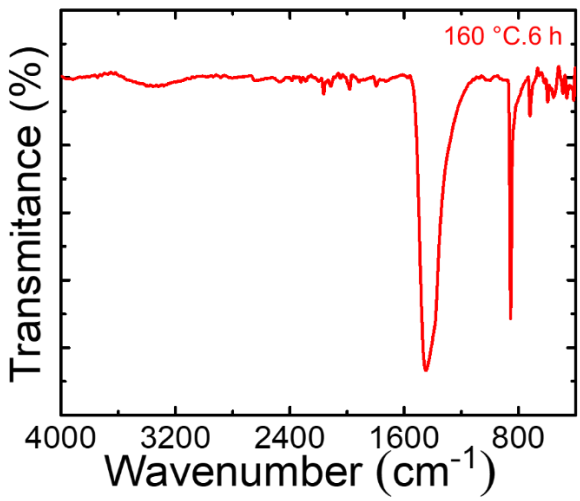

Figure S9. FTIR spectra of $Zn_{1-x}Cd_xS$ PNP/ ZnO NR160 photoanode.

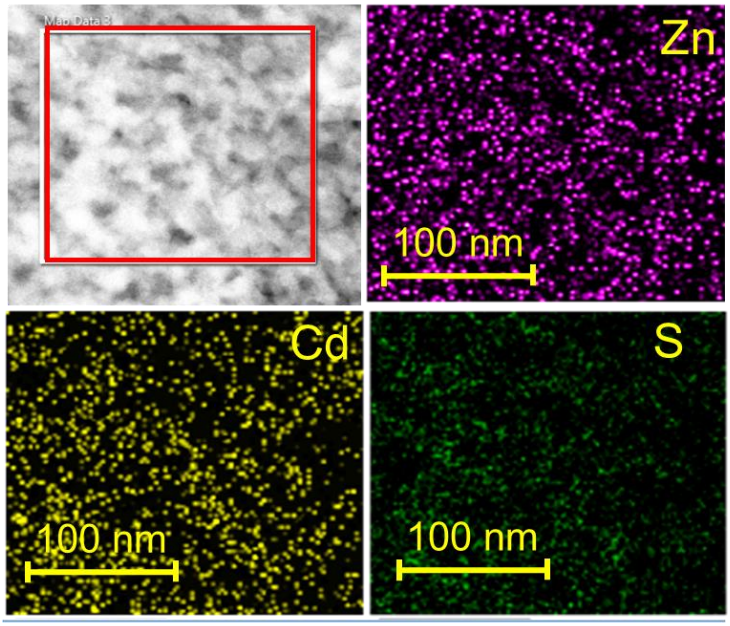

Element	Line Type	Wt%	Atomic %
S	K series	15.58	38.18
Zn	K series	2.26	3.21
Cd	L series	77.05	58.71
Total:		100.00	100.00

Figure S10. EDS images of selectivtive $Zn_{1-x}Cd_xS$ PNP of $Zn_{1-x}Cd_xS$ PNP/ZnO NR160 photoanode.

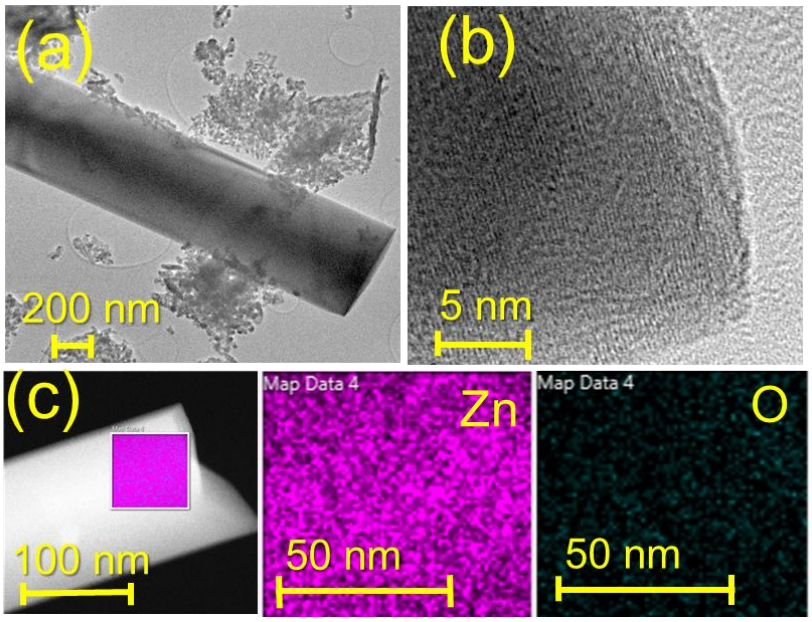

Figure S11. (a) TEM, (b) HRTEM and (c) EDS mapping images of selectivtive ZnO NR of $Zn_{1-x}Cd_xS$ PNP/ ZnO NR160 photoanode.

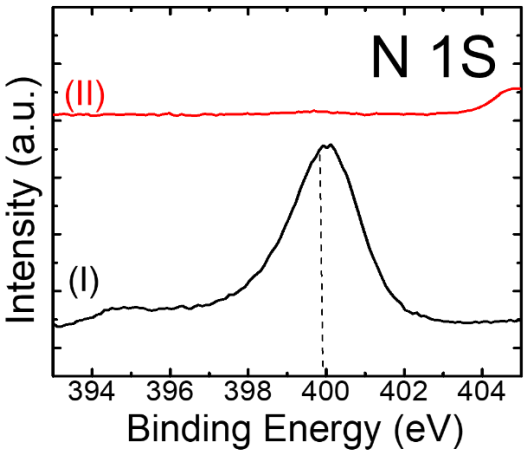

Figure S12. XPS spectra of (I) $ZnS(en)_{0.5}$ NP -2 electrode and (II) $Zn_{1-x}Cd_xS$ PNP/ ZnO NR160 photoanode for N1 S.

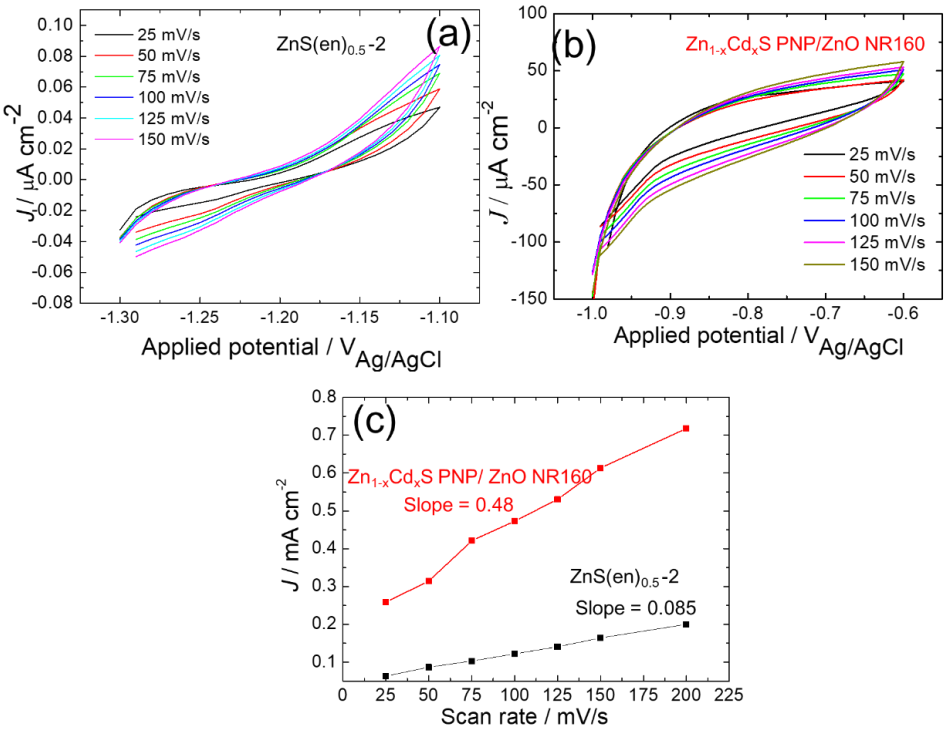

Figure S13. Cyclic voltammetry of (a) inorganic–organic hybrid $ZnS(en)_{0.5}$ NP-2 (b) $Zn_{1-x}Cd_xS$ PNP/ZnO NR160 photoanodes at different scan rates, and (c) relative electrochemical surface area.

The cyclic voltammetry (CV) was carried out to understand the electrochemically active surface area (ESCA). Figure S13(a-c) shows the ESCA surface of the $ZnS(en)_{0.5}$ NP -2 and ZnO NR/$Zn_{1-x}Cd_xSe$ NP180 photoanode measured at the applied potential. -1.2 to 0.4 V *vs*. Ag/AgCl in 0.25 M Na_2S + 0.35 M Na_2SO_3 electrolyte solution. The active surface areas of ZnO NR/$Zn_{1-x}Cd_xSe$ NP photoanodes were obtained from the different CV scan rates (25, 50, 75, 100, 125, and 150 mVs^{-1}) with respect to the capacitive current. The $ZnS(en)_{0.5}$ -2 electrode exhibits a lower slope value (0.085) compared to the ZnO NR/$Zn_{1-x}Cd_xS$ NP160 photoanode. The smaller surface area is due to the absence of the porous structure. However, after Cd^{2+} ion exchange, the optimized photoanode provides a larger surface area due to porous structure and optimized growth of ZnO NR. [1]

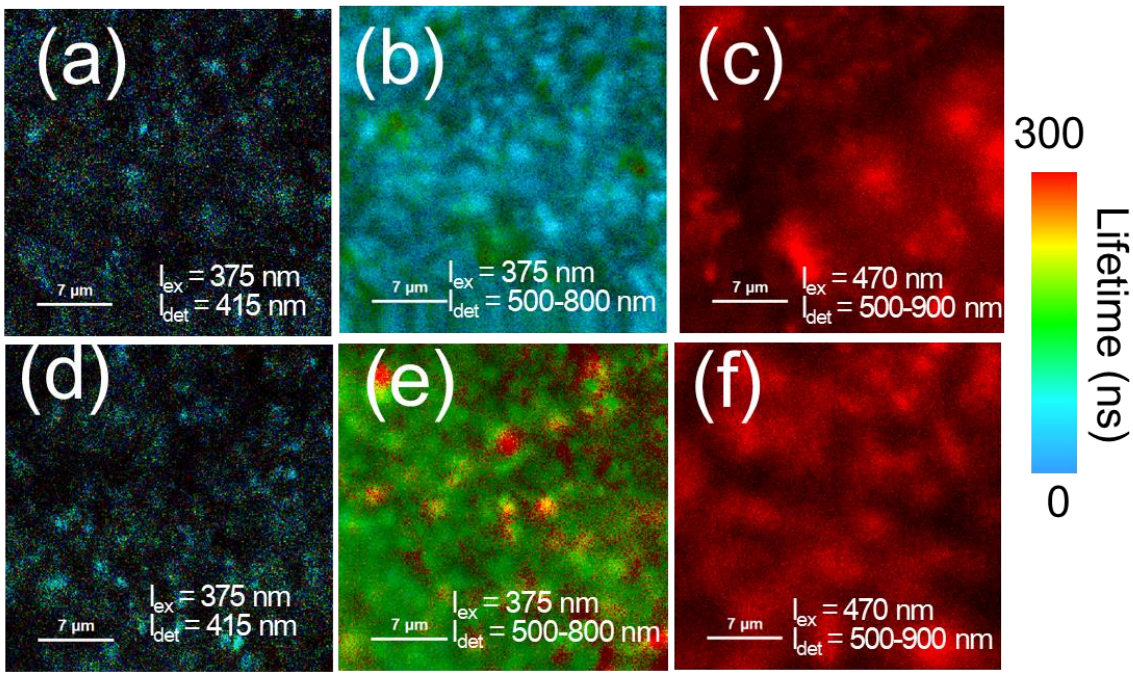

Figure S14. (a-f) PL lifetime images of t (a-c) $Zn_{1-x}Cd_xS$ PNP/ZnO NR160 and (d-f) $Zn_{1-x}Cd_xS$ PNP/ZnO NR180 photoanodes after 375 and 470 nm laser excitation, detected at (a, d) 415 and (b, e) 500-800 nm, respectively. (c, f) PL lifetime images were detected at 500-900 nm after a 470 nm laser excitation.

Photocorrosion process of $Zn_{1-x}Cd_xS$ PNP /ZnO NR 160 photoanode

The reason for hydrogen evolution drops with time with respect to time. Under one sun illumination, the $Zn_{1-x}Cd_xS$ PNP /ZnO photoanode generates the charge carriers. Among them, the photogenerated electron goes to the counter electrode and photogenerated holes go to the surface of photoanodes. Further, these photogenerated holes (h^+) react with SO_3^{2-} and S^{2-} and form S_2^{2-} and $S_2O_3^{2-}$. [2, 3] However, the $Zn_{1-x}Cd_xS$ is unstable in Na_2S and Na_2SO_3 aqueous electrolytes with a solution containing S^{2-} and/or SO_3^{2-}.[4-5]

$$Zn_{1-x}Cd_xS\ PNP/ZnO\ NR + h\upsilon \rightarrow Zn_{1-x}Cd_xS\ PNP/ZnO\ NR\ (e^- + h^+) \quad (1)$$

$$2H_2O + 2e^- \rightarrow H_2 + 2OH^- \quad (2)$$

$$SO_3^{2-} + H_2O + 2h^+ \rightarrow SO_4^{2-} + 2H^+ \quad (3)$$

$$2S^{2-} + 2h^{+} \rightarrow S_2^{2-} \quad (4)$$

$$S_2^{2-} + SO_3^{2-} \rightarrow S_2O_3^{2-} + S^{2-} \quad (5)$$

$$SO_3^{2-} + S^{2-} + 2h^{+} \rightarrow S_2O_3^{2-} \quad (6)$$

However, the main reason for the photocorrosion is not only excess photoinduced holes present on the sulfide surface, which causes the serious photocorrosion of $Zn_{1-x}Cd_xS$ PNP/ZnO NR photoanodes. [6]

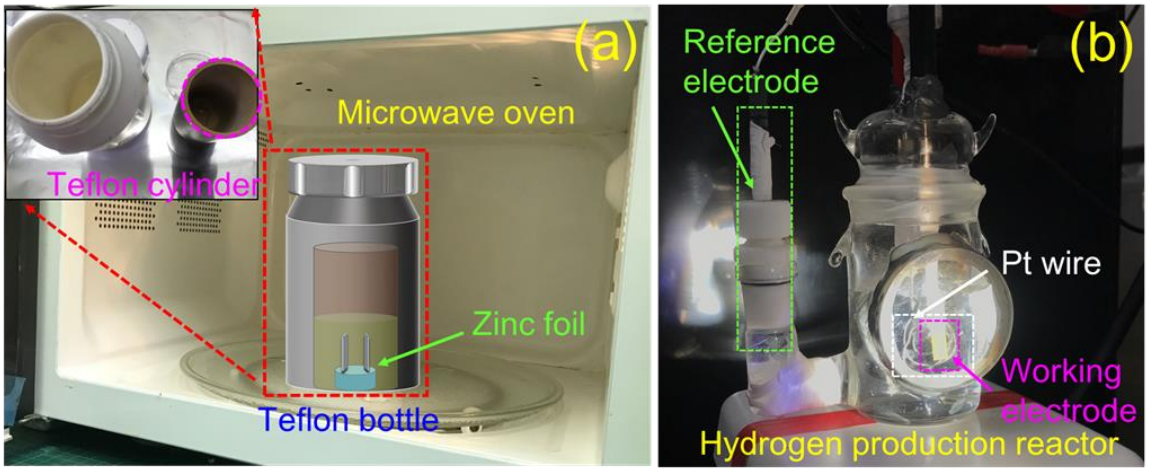

Figure S15. Digital photograph of (a) synthesis of inorganic–organic hybrid $ZnS(en)_{0.5}$ NP electrode by MW method and (b) hydrogen production reactor setup.

References

(1) Patil, R.P.; Mahadik, M.A.; Bae, H.S.; Chae, W.S.; Choi, S.H.; Jang, J.S. Porous $Zn_{1-x}Cd_xS$ Nanosheets/ZnO Nanorod Heterojunction Photoanode *via* Self-Templated and Cadmium Ions Exchanged Conversion of $ZnS(HDA)_{0.5}$ Nanosheets/ZnO Nanorod. *Chem. Eng. J.* **2020**, *402*, 26153.

(2) Wang, G.; Yang, X.; Qian, F.; Zhang, J. Z.; Li, Y. Double-sided CdS and CdSe Quantum Dot Co-sensitized ZnO Nanowire Arrays for Photoelectrochemical Hydrogen Generation. *Nano lett.* **2010**, *10*, 1088-1092.

(3) Chen, Y.; Wang, L.; Wang, W.; Cao, M. Enhanced Photoelectrochemical Properties of ZnO/ZnSe/CdSe/$Cu_{2-x}Se$ Core–Shell Nanowire Arrays Fabricated by Ion-replacement Method. *Appl. Catal. B,* **2017**, *209*, 110-117.

(4) Wang, M.; Shen, S.; Li, L.; Tang, Z.; Yang, J. Effects of Sacrificial Reagents on Photocatalytic Hydrogen Evolution Over Different Photocatalysts. *J. Mater. Sci.* **2017**, *52*, 5155-5164.

(5) Gomathisankar, P.; Hachisuka, K.; Katsumata, H.; Suzuki, T.; Funasaka, K.; Kaneco, S. Photocatalytic Hydrogen Production with CuS/ZnO From Aqueous Na_2S+ Na_2SO_3 Solution. *Int. J. Hydrog. Energy*, **2013**, *38*, 8625-8630.

(6) Ning, X.; Lu, G. Photocorrosion Inhibition of CdS-Based Catalysts for Photocatalytic Overall Water Splitting. *Nanoscale*, **2020**, *12*, 1213-1223.